Editors' Suggestion

Controlling the Spatial Profile and Energy Landscape of Organic Polariton Condensates in Double-Dye Cavities

Anton D. Putintsev,[1,*] Kirsty E. McGhee,[2] Denis Sannikov,[1] Anton V. Zasedatelev,[1] Julian D. Töpfer,[1] Till Jessewitsch,[3] Ullrich Scherf,[3] David G. Lidzey,[2] and Pavlos G. Lagoudakis[1,†]

[1]*Hybrid Photonics Laboratory, Skolkovo Institute of Science and Technology, Territory of Innovation Center Skolkovo, Bolshoy Boulevard 30, Building 1, 121205 Moscow, Russia*

[2]*Department of Physics and Astronomy, University of Sheffield, Hicks Building, Hounsfield Road, Sheffield S3 7RH, United Kingdom*

[3]*Macromolecular Chemistry Group and Institute for Polymer Technology, Bergische Universität Wuppertal, Wuppertal 42119, Germany*

(Received 3 March 2023; revised 21 July 2023; accepted 20 September 2023; published 30 October 2023)

The development of high-speed, all-optical polariton logic devices underlies emerging unconventional computing technologies and relies on advancing techniques to reversibly manipulate the spatial extent and energy of polartion condensates. We investigate active spatial control of polariton condensates independent of the polariton, gain-inducing excitation profile. This is achieved by introducing an extra intracavity semiconductor layer, nonresonant to the cavity mode. Partial saturation of the optical absorption in the uncoupled layer enables the ultrafast modulation of the effective refractive index and, through excited-state absorption, the polariton dissipation. Utilizing an intricate interplay of these mechanisms, we demonstrate control over the spatial profile, density, and energy of a polariton condensate at room temperature.

DOI: 10.1103/PhysRevLett.131.186902

The ability to shape the potential energy landscape to confine polariton condensates into geometrically arranged regular or arbitrary arrays underpins various applications, such as topological polaritonics [1–4], lattice simulators [5–8], and neural networks [9,10], and allows for the investigation of fundamental physics [11–13]. An essential part in all these studies is to have tools and techniques to control the polariton energy landscape that is usually achieved by means of lithographic or optical methods. The lithographic approach allows for the local control of the photonic component of the system by a straightforward lithographic modulation of the cavity length [14], deep etching of micropillars into the structure [15,16], metal films deposition on the surface of a grown microcavity structure [17], or by exploiting natural photonic disorder potentials present in microcavities due to growth related defects [18–20]. All-optical methods to control the energy landscape of polaritons offer higher flexibility in customizing its shape while circumventing inherent disorder. Whether it is a single Gaussian pump or an array of pumps geometrically arranged in multiple-spot configurations and lattices, forming either ballistically expanding [21] or trapped polariton condensates [22], one exploits a localized blueshift effect that at the same time induces additional gain in the system.

Manipulating polariton potentials through additional gain-inducing optical excitation adds a real-valued component to the interaction between polariton condensates that strongly affects the energy of the condensate. An alternative approach of utilizing local control of polaritons through dissipation via ion implantation was recently proposed [23,24] to control the coupling between nearest neighbors in arrays of polariton condensates. Furthermore, it would be desirable to introduce local dissipation in a reversible manner that can enable both *ad hoc* landscape engineering of polariton condensates and real-time control over the coupling between nearest neighbor condensates without adding gain to the system. Despite the potential of such an approach, to date, control of local polariton dissipation has remained illusive both in organic and inorganic microcavities.

In this Letter, we experimentally demonstrate ultrafast and reversible manipulation of the condensate energy and density by shaping both the local potential and dissipation in the real space at room temperature. We utilize a double-dye organic microcavity, depicted on the top panel of Fig. 1, that recently was proposed as a new platform for optically controlled polariton condensate lattices operational at room temperature [25]. The microcavity includes one layer of strongly coupled BODIPY-Br dye molecules and a blue-detuned uncoupled layer of the copolymer BN-PFO. We demonstrate polariton condensation under nonresonant optical excitation and, by simultaneous excitation of the uncoupled layer, tuning of the condensate energy up to 8 meV. Excited-state absorption of the uncoupled molecular dyes results in increasing losses for polaritons. In tandem with the energy blueshifts, due to the decrease of the intracavity effective refractive index at the energy of the lower polariton mode, excited-state absorption allows us to control the spatial profile of a polariton condensate.

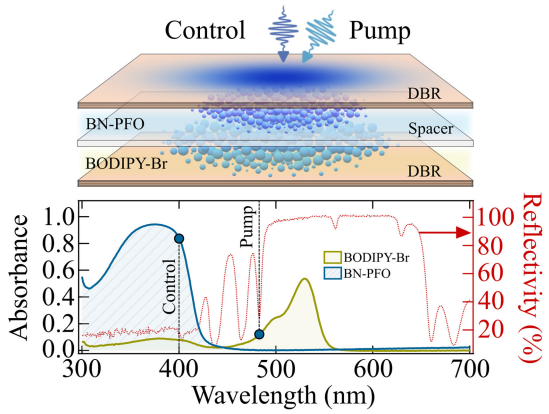

FIG. 1. Top: schematic of a double-dye organic microcavity. Bottom: the absorbance spectra of the uncoupled BN-PFO dye molecules and the coupled BODIPY-Br dye molecules (left axis) and the reflectivity spectrum of the structure (right axis). Black vertical dashed lines indicate the spectral tuning of pump and control excitation beams.

Polariton density-dependent energy blueshifts in semiconductor microcavities are omnipresent at high excitations and usually corroborate evidence of strong coupling. However, the mechanism behind blueshifts in crystalline, usually inorganic, and noncrystalline, usually organic, semiconductors is different. In the first case, the blueshift is predominantly due to the Coulombic exchange interaction between Wannier-Mott excitons [26,27], whereas in the latter case of Frenkel excitons, it is due to the saturation of molecular optical transitions. It was recently shown that the blueshifts in molecular-dye microcavities are not only due to the quenching of the Rabi splitting but predominantly due to changes of the intracavity refractive index from the saturation of both coupled and uncoupled molecules [28]. Here, we utilize a structure design that allows us to decouple these mechanisms.

The structure consists of two layers of different organic materials embedded within the microcavity. One 285-nm-thick layer of the molecular dye BODIPY-Br and one 170-nm-thick layer of the conjugated polymer BN-PFO, separated by an inert polyvinyl alcohol spacer layer of 60-nm thickness. The organic layers are sandwiched in between a bottom SiO_2/Nb_2O_5 and a top SiO_2/TiO_2 distributed Bragg reflector (DBR), as shown schematically in the top panel of Fig. 1, resulting in a quality factor of ≈920; see McGhee *et al.* (2023) [25] for a complete description and characterization of the microcavity structure. The absorption spectra of the BODIPY-Br and BN-PFO layers, and the reflectivity spectrum of the full cavity, are shown in the bottom panel of Fig. 1. Despite the presence of the weakly coupled, blue-detuned to the cavity mode, BN-PFO absorber in the microcavity, the BODIPY-Br layer couples strongly to the bare cavity mode exhibiting a Rabi splitting (Ω) of 103 meV [25]. The cavity exhibits a small range of available detunings (δ), and throughout this study the detuning was kept constant at ≈ -90 meV, with exciton and photon fractions, $|X_{e,p}|^2 = [1 \pm \delta/\sqrt{(\delta^2 + \Omega^2)}]/2$, of 0.17 and 0.83, respectively. These two layers are independently excited using a two color optical excitation beam configuration; see dashed black lines in the bottom panel of Fig. 1.

We examine whether polariton condensation is achievable in the double-dye microcavity using nonresonant pulsed optical excitation of 2 ps temporal width tuned at the first Bragg minimum of the reflectivity stop band: 485 nm. Figure 2(a) shows a pump power dependence of polariton photoluminescence (PL) vs the absorbed pump fluence on the bottom horizontal axis. The onset to nonlinear emission is defined as the crossing of the two black dashed lines in Fig. 2(a), $P_{\mathrm{th}} \approx 400\ \mu\mathrm{J/cm^2}$, see bottom horizontal axis. At P_{th}, we observe a concomitant collapse of the photoluminescence linewidth, from 8 to 1.8 meV, and a blueshift of the emission energy, see Fig. 2(b). Each point on the plots of Figs. 2(a) and 2(b) is derived from a dispersion image obtained under a single excitation pulse, whose fluence is simultaneously recorded. We note that the slope difference in the blueshift below and after condensation threshold in Fig. 2(b) originates from the interplay between intermolecular energy transfer between excitons of different alignment with respect to the excitation beam and stimulated relaxation to the ground-polariton state. Above threshold, the rate of the latter mechanism surpasses that of intermolecular energy transfer resulting in a higher rate of Rabi-splitting quenching from molecules aligned in parallel with the pump beam [28]. In Fig. 2(c), we show the single-shot dispersion image of the lower polariton branch at $P_{\mathrm{pump}} \sim 2 \times P_{\mathrm{th}}$. The emission is blueshifted by 2.5 meV from the linear dispersion that is indicated with a white dotted line. Following the formalism of Ref. [28], we can estimate the two contributions to the blueshift from the saturation of the molecular optical transitions for this structure (see also Supplemental Material, Sec. I [29]). We obtain that the dominant component of the blueshift, 1.84 meV, is due to the effective refractive index renormalization, and 0.66 meV is due to the vacuum Rabi-splitting quenching. The observed threshold for polariton condensation is similar to that observed previously for BODIPY-family dye filled microcavities [28,32–35], indicating that the presence of the BN-PFO absorber in the cavity does not affect the dynamics of polariton condensation under nonresonant excitation at 485 nm.

To explore the effect of saturation of the molecular transitions of the second layer of molecular dyes on the polariton condensate, we introduce a second optical excitation "control" beam of 500 fs temporal width and resonant with the absorption of BN-PFO at 400 nm, see the bottom panel of Fig. 1. We keep the pump fluence of the 485-nm beam constant at twice the condensation threshold, $2 \times P_{\mathrm{th}}$, and perform a fluence dependence of the control beam at zero time delay between pump and control pulses. For a

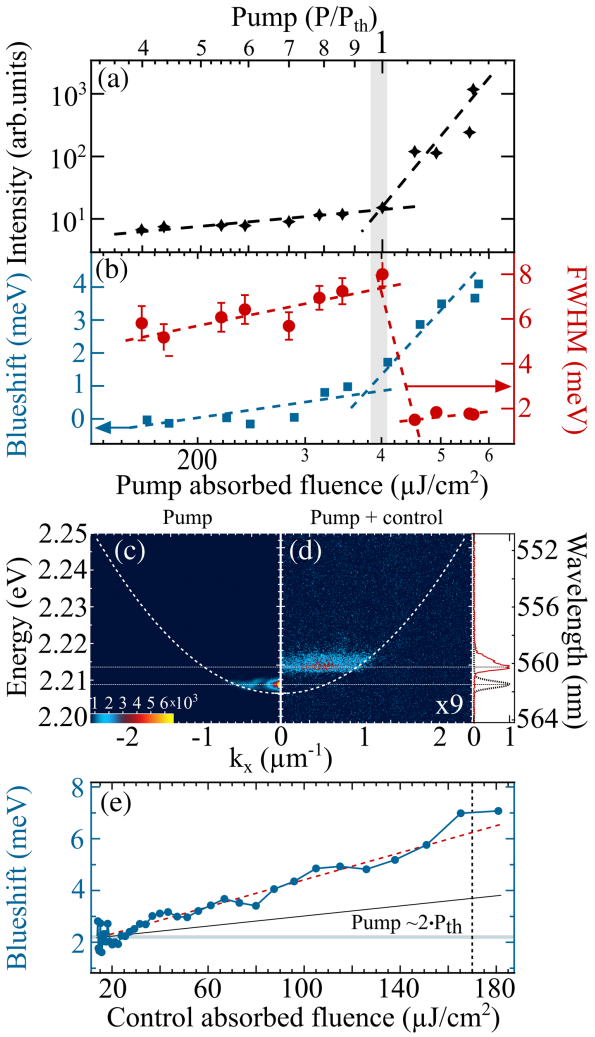

FIG. 2. Polariton photoluminescence (a) intensity, (b) blueshift of the PL spectrum in blue squares (left axis), and the corresponding linewidth in red dots (right axis) measured at full width at half maximum (FWHM) vs pump absorbed fluence (bottom axis) and pump threshold (top axis). The vertical gray shaded line indicates the condensation threshold. Normalized single-shot dispersion images recorded at $\sim 2 \times P_{\mathrm{th}}$ in the (c) absence and (d) presence of the control beam. The white dashed lines indicate the linear dispersion, and $\times 9$ is the scale factor for a normalized color bar. The right side of (d) shows the corresponding spectra in black dotted and red solid lines, respectively. (e) Polariton blueshift vs the control beam absorbed fluence. The horizontal solid gray line indicates the blueshift of the polariton condensate at $\sim 2 \times P_{\mathrm{th}}$ in the absence of the control beam. The dashed red line is a linear fit to the blueshift dependence. The black solid line is the estimated blueshift due to effective refractive index change at the energy of the polariton condensate due to saturation of the molecular optical transitions. The difference in the slope between the black solid and dashed red dependencies of the blueshift is attributed to the excited-state absorption.

control beam fluence of $\approx 250\ \mu\mathrm{J/cm^2}$, BN-PFO absorbs $\approx 180\ \mu\mathrm{J/cm^2}$, and BODIPY-Br absorbs $\approx 2\ \mu\mathrm{J/cm^2}$. The latter corresponds to $\approx 2\%$ of the required absorbed fluence for polariton condensation of BODIPY-Br when pumped at 400 nm [35], which brings a nondiscernible effect to the dynamics of the condensate. Under these excitation conditions, we perform single-pulse dispersion imaging, shown in Fig. 2(d), and observe an additional 5 meV blueshift, in the presence of the control pulse. The right panel of Fig. 2(d) shows the PL spectra of the condensate in the presence and absence of the control beam. Evidently the linewidth of the condensate in the presence of the control beam is broadened, indicating the onset of dissipation due to excited-state absorption from the uncoupled excitons in BN-PFO. Figure 2(e) shows the dependence of the blueshift on the absorbed fluence of the control beam. The energy shift dependence on the change of effective refractive index is given by $\Delta E \cong -E_c(\Delta n/n_{\mathrm{eff}})$, where ΔE is the energy shift, E_c is the bare cavity optical resonance, and Δn is the change of the effective cavity refractive index n_{eff} [28]. For the density of BN-PFO molecules $n_0 \approx 1.2 \pm 0.2\ \mathrm{g/cm^3}$, we can estimate the negative change of the intracavity effective refractive index at the energy of the polariton condensate using the Kramers-Kronig relation and plot the corresponding energy shift with a solid black line in Fig. 2(e) (see Supplemental Material, Sec. I [29]). The difference between the estimated blueshift and the experimental observation is attributed to excited-state absorption from the molecules of BN-PFO. Excited-state absorption from BN-PFO has a broadband resonance that overlaps with the polariton emission [25]. Transient reflectivity measurements under saturation of BN-PFO revealed that excited-state absorption results in an energy shift of the polariton mode due to changes of the effective refractive index [25].

We investigate the transient dynamics of the observed blueshifts by scanning the time delay between the pump and control pulses and recording the dispersion image of the PL for each excitation pulse. We keep the pump fluence constant at $2 \times P_{\mathrm{th}}$ and the absorbed control beam fluence at $\approx 170\ \mu\mathrm{J/cm^2}$, see vertical dashed line in Fig. 2(e). Figure 3(a) shows the temporal dependence of the blueshift vs pump control beam time delay. The transient decay of the blueshift can be fitted with a biexponential decay. The fast component has the same characteristic time, ≈ 1.7 ps, as the rise dynamics and is dominated by exciton-exciton annihilation in the BN-PFO, resolution limited here by the temporal width of the pump pulses [36]. The slow component, ≈ 56 ps, corresponds to the recombination dynamics of the excitons in BN-PFO in the absence of nonlinear recombination mechanisms. Figure 3(b) shows the corresponding temporal dynamics of the condensate PL intensity. Here, we observe strong quenching of the polariton density at zero time delay that follows approximately the same characteristic times of the blueshift. The depletion of polariton density indicates the onset of strong polariton dissipation in the presence of a far blue-detuned and spatially separated exciton reservoir. In the absence of intermolecular energy transfer between the two molecular

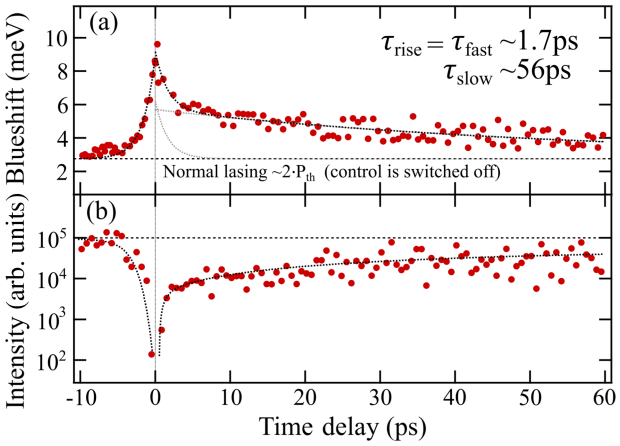

FIG. 3. Pump control time delay scan: the pump beam fluence is fixed at $\sim 2 \times P_{th}$ and the control beam absorbed fluence at $\approx 170\ \mu J/cm^2$; positive time delay corresponds to earlier arrival of the control pulse. (a) Blueshift dependence on the time delay, exhibiting a double exponential decay with two components shown by gray dashed lines. (b) Polariton PL intensity dependence on the time delay, exhibiting quenching of emission with the same characteristic times of the blueshift dependence. The horizontal dashed lines indicate the polariton blueshift (a) and intensity (b) at $\sim 2 \times P_{th}$ in the absence of the control beam; the vertical lines indicate the zero time delay.

dyes, the dissipation of polaritons is attributed to excited-state absorption from the BN-PFO molecules [25].

It is apparent that, beyond the control over locally induced blueshifts, excited-state absorption induces strong local dissipation that is both tunable and reversible. We utilize spatial modulation of the control beam to demonstrate *ad hoc* localization of the polariton condensate. We expand the pump to a ~30 μm Gaussian beam at $\approx 2 \times P_{th}$ above the condensation threshold and use a spatial light modulator to shape the control beam into a ring of ~20 μm in diameter, as shown schematically in Fig. 4(a). Figure 4(b) shows the disorder-limited spatial profile of the polariton condensate in the absence of the control beam; the top panel shows the PL intensity cross section obtained from the horizontal dotted line in Fig. 4(b). Figure 4(c) shows the polariton PL in the presence only of the control beam with an absorbed energy of ~500 pJ due to the residual absorption of BODIPY-Br at 400 nm and reabsorption of BN-PFO emission by the BODIPY-Br; see Supplemental Material, Sec. II [29]. The top panel of Fig. 4(c) shows the corresponding PL intensity across a horizontal cross section. Figure 4(d) shows the respective polariton condensate PL in the presence of both pump and control beams, showing strong localization of the polariton condensate. By tuning the absorbed fluence of the control beam, we can simultaneously control both the extent of the condensate and its respective blueshift. Figures 4(e) and 4(f) show the spatial width, blueshift, and condensate PL intensity vs the control absorbed energy, obtained from a single-pulse spectrally resolved imaging of the condensate real-space PL across a vertical cross section, annotated with a blue dashed line in Fig. 4(b). Figure 4(f) shows that the intensity of the condensate is monotonically depleted with increasing the control beam absorbed energy. This

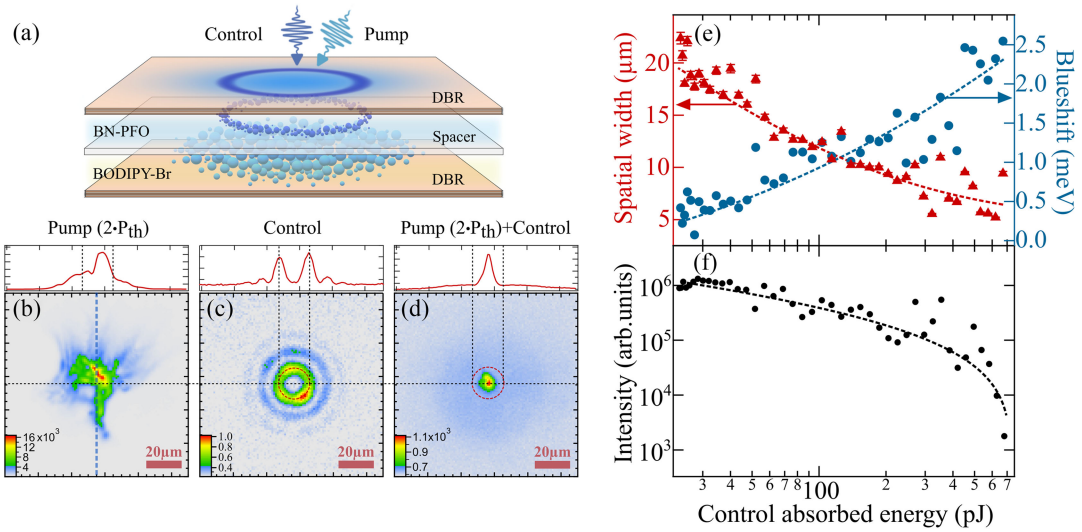

FIG. 4. (a) Schematic of the Gaussian pump and ring-shaped control excitation beams. The control beam saturates the uncoupled BN-PFO layer at 400 nm, and the pump beam nonresonantly injects a polariton condensate in the strongly coupled BODIPY-Br layer at 485 nm. (b) Single-shot real-space emission image of a polariton condensation at $2 \times P_{th}$. (c) Averaged over 100 realizations real-space emission image of the PL from BODIPY-Br layer excited by ~500 pJ absorbed energy of the ring-shaped control beam. (d) Single-shot real-space emission image of the polariton condensate of (b) in the presence of the ring-shaped control pulse (red dashed circle) of (c) at zero time delay. (e) The dependence of the spatial width (red markers, left axis) of the polariton condensate emission across the vertical blue dashed line of (b) and the corresponding blueshift (blue markers, right axis) from the center of the ring of (d) vs the control pulse absorbed energy. (f) The polariton emission intensity dependence from the center of the ring of (d) vs the control pulse absorbed energy. Blue, red, and black dashed lines on (e) and (f) are guides to the eye.

dependence is attributed to the dominant role of a locally induced dissipation that out competes any pump- or control-beam-induced gain. Whereas there is spectroscopic evidence of a localized blueshift across the axicon-shaped control beam area in the presence of a polariton condensate (see Supplemental Material, Sec. III [29]), the complete quenching of polariton emission across the axicon [see Fig. 4(d)] obscures any spectroscopic signatures of spatial trapping, unlike the optical trapping observed in inorganic microcavities [37]. Thus, we can confidently state that tuning over the spatial width and energy of the condensate [see Fig. 4(e)] is predominantly driven by the strength of the dissipation induced by the control beam.

In conclusion, we investigate reversible spatial control of polariton energy shifts and local dissipation by introducing an extra intracavity semiconductor layer, whose optical absorption transition is nonresonant to the cavity mode. By using a control beam to partially saturate the intracavity layer, we modify the effective refractive index of the cavity (and thus cavity path-length) and also introduce an additional excited-state absorption, with both effects allowing us to generate a controllable, ultra-fast blueshift of the polariton condensate energy. Using a spatial light modulator, we project a circular pattern onto the cavity which results in a local blueshift of the energy of the lower polariton branch. This results in the direct control over the spatial profile of a polariton condensate at room temperature. Our study realizes previously unexplored physical mechanisms for the reversible manipulation of the spatial profile and energy of polariton condensates in organic microcavities. Our work will enable studies of new physical regimes and will allow new tools to be realized for the controlled preparation of states and manipulation of various excitations in gain-dissipative systems. We believe the methodology outlined here is likely to advance the development of new types of polaritonic devices, including high-speed, all-optical polariton logic and simulator devices at ambient conditions.

This work was supported by the Russian Science Foundation (RSF) Grant No. 23-72-00059. K. E. M. and D. G. L. thank the U.K. EPSRC for support via the program Grant "Hybrid Polaritonics" (EP/M025330/1). K. E. M. thanks the EPSRC for support through Grant No. EP/R513313/1.

*Corresponding author: anton.putintsev@skoltech.ru
†Corresponding author: p.lagoudakis@skoltech.ru

[1] N. H. M. Dang *et al.*, Realization of polaritonic topological charge at room temperature using polariton bound states in the continuum from perovskite metasurface, Adv. Opt. Mater. **10**, 2102386 (2022).
[2] V. Ardizzone *et al.*, Polariton Bose–Einstein condensate from a bound state in the continuum, Nature (London) **605**, 447 (2022).
[3] P. St-Jean *et al.*, Measuring topological invariants in a polaritonic analog of graphene, Phys. Rev. Lett. **126**, 127403 (2021).
[4] V. Kravtsov *et al.*, Nonlinear polaritons in a monolayer semiconductor coupled to optical bound states in the continuum, Light Sci. Appl. **9**, 56 (2020).
[5] A. Kavokin, T. C. H. Liew, C. Schneider, P. G. Lagoudakis, S. Klembt, and S. Hoefling, Polariton condensates for classical and quantum computing, Nat. Rev. Phys. **4**, 435 (2022).
[6] N. G. Berloff, M. Silva, K. Kalinin, A. Askitopoulos, J. D. Töpfer, P. Cilibrizzi, W. Langbein, and P. G. Lagoudakis, Realizing the classical *XY* Hamiltonian in polariton simulators, Nat. Mater. **16**, 1120 (2017).
[7] A. Amo and J. Bloch, Exciton-polaritons in lattices: A nonlinear photonic simulator, C.R. Phys. **17**, 934 (2016).
[8] I. Carusotto and C. Ciuti, Quantum fluids of light, Rev. Mod. Phys. **85**, 299 (2013).
[9] D. Ballarini *et al.*, Polaritonic neuromorphic computing outperforms linear classifiers, Nano Lett. **20**, 3506 (2020).
[10] R. Mirek *et al.*, Neuromorphic binarized polariton networks, Nano Lett. **21**, 3715 (2021).
[11] I. Gnusov, S. Harrison, S. Alyatkin, K. Sitnik, J. Töpfer, H. Sigurdsson, and P. Lagoudakis, Quantum vortex formation in the "rotating bucket" experiment with polariton condensates, Sci. Adv. **9**, eadd1299 (2023).
[12] Y. del Valle-Inclan Redondo, C. Schneider, S. Klembt, S. Höfling, S. Tarucha, and M. D. Fraser, Optically driven rotation of exciton–polariton condensates, Nano Lett. **23**, 4564 (2023).
[13] J. D. Töpfer, H. Sigurdsson, L. Pickup, and P. G. Lagoudakis, Time-delay polaritonics, Commun. Phys. **3**, 2 (2020).
[14] O. El Daïf, A. Baas, T. Guillet, J.-P. Brantut, R. Idrissi Kaitouni, J. L. Staehli, F. Morier-Genoud, and B. Deveaud, Polariton quantum boxes in semiconductor microcavities, Appl. Phys. Lett. **88**, 061105 (2006).
[15] M. Obert, J. Renner, A. Forchel, G. Bacher, R. André, and D. Le Si Dang, Nonlinear emission in II–VI pillar microcavities: Strong versus weak coupling, Appl. Phys. Lett. **84**, 1435 (2004).
[16] D. Bajoni, P. Senellart, E. Wertz, I. Sagnes, A. Miard, A. Lemaître, and J. Bloch, Polariton laser using single micropillar GaAs-GaAlAs semiconductor cavities, Phys. Rev. Lett. **100**, 047401 (2008).
[17] N. Y. Kim *et al.*, GaAs microcavity exciton-polaritons in a trap, Phys. Status Solidi (b) **245**, 1076 (2008).
[18] R. Spano *et al.*, Coherence properties of exciton polariton OPO condensates in one and two dimensions, New J. Phys. **14**, 075018 (2012).
[19] J. M. Zajac and W. Langbein, Structure and zero-dimensional polariton spectrum of natural defects in GaAs/AlAs microcavities, Phys. Rev. B **86**, 195401 (2012).
[20] V. D. Kulakovskii, A. V. Larionov, S. I. Novikov, S. Höfling, Ch. Schneider, and A. Forchel, Bose-Einstein condensation of exciton polaritons in high-Q planar microcavities with GaAs quantum wells, JETP Lett. **92**, 595 (2010).

[21] S. Alyatkin, J. D. Töpfer, A. Askitopoulos, H. Sigurdsson, and P. G. Lagoudakis, Optical control of couplings in polariton condensate lattices, Phys. Rev. Lett. **124**, 207402 (2020).
[22] M. Wei, W. Verstraelen, K. Orfanakis, A. Ruseckas, T. C. H. Liew, I. D. W. Samuel, G. A. Turnbull, and H. Ohadi, Optically trapped room temperature polariton condensate in an organic semiconductor, Nat. Commun. **13**, 7191 (2022).
[23] M. D. Fraser, H. Hoe Tan, Y. del Valle Inclan Redondo, H. Kavuri, E. A. Ostrovskaya, C. Schneider, S. Höfling, Y. Yamamoto, and S. Tarucha, Independent tuning of exciton and photon energies in an exciton–polariton condensate by proton implantation-induced interdiffusion, Adv. Opt. Mater. **11**, 2201569 (2023).
[24] K. P. Kalinin and N. G. Berloff, Toward arbitrary control of lattice interactions in nonequilibrium condensates, Adv. Quantum Technol. **3**, 1900065 (2020).
[25] K. E. McGhee *et al.*, Ultrafast optical control of polariton energy in an organic semiconductor microcavity, Adv. Opt. Mater. **11**, 2300262 (2023).
[26] M. Vladimirova, S. Cronenberger, D. Scalbert, K. V. Kavokin, A. Miard, A. Lemaître, J. Bloch, D. Solnyshkov, G. Malpuech, and A. V. Kavokin, Polariton-polariton interaction constants in microcavities, Phys. Rev. B **82**, 075301 (2010).
[27] Y. Sun, P. Wen, Y. Yoon, G. Liu, M. Steger, L. N. Pfeiffer, K. West, D. W. Snoke, and K. A. Nelson, Bose-Einstein condensation of long-lifetime polaritons in thermal equilibrium, Phys. Rev. Lett. **118**, 016602 (2017).
[28] T. Yagafarov *et al.*, Mechanisms of blueshifts in organic polariton condensates, Commun. Phys. **3**, 18 (2020).
[29] See Supplemental Material at http://link.aps.org/supplemental/10.1103/PhysRevLett.131.186902 for the complementary experimental datasets and extended analysis, which includes Refs. [30,31].
[30] F. Schindler, J. Jacob, A. C. Grimsdale, U. Scherf, K. Müllen, J. M. Lupton, and J. Feldmann, Counting chromophores in conjugated polymers, Angew. Chem., Int. Ed. **44**, 1520 (2005).
[31] A. J. Musser *et al.*, Intermolecular states in organic dye dispersions: Excimers vs. aggregates, J. Mater. Chem. C **5**, 8380 (2017).
[32] A. Putintsev, A. Zasedatelev, K. E. McGhee, T. Cookson, K. Georgiou, D. Sannikov, D. G. Lidzey, and P. G. Lagoudakis, Nano-second exciton-polariton lasing in organic microcavities, Appl. Phys. Lett. **117**, 123302 (2020).
[33] K. E. McGhee *et al.*, Polariton condensation in an organic microcavity utilising a hybrid metal-DBR mirror, Sci. Rep. **11**, 20879 (2021).
[34] D. Sannikov, T. Yagafarov, K. Georgiou, A. Zasedatelev, A. Baranikov, L. Gai, Z. Shen, D. Lidzey, and P. Lagoudakis, Room temperature broadband polariton lasing from a dye-filled microcavity, Adv. Opt. Mater. **7**, 1900163 (2019).
[35] T. Cookson *et al.*, A yellow polariton condensate in a dye filled microcavity, Adv. Opt. Mater. **5**, 1700203 (2017).
[36] H. Marciniak, M. Teicher, U. Scherf, S. Trost, T. Riedl, M. Lehnhardt, T. Rabe, W. Kowalsky, and S. Lochbrunner, Photoexcitation dynamics in polyfluorene-based thin films: Energy transfer and amplified spontaneous emission, Phys. Rev. B **85**, 214204 (2012).
[37] A. Askitopoulos, H. Ohadi, A. V. Kavokin, Z. Hatzopoulos, P. G. Savvidis, and P. G. Lagoudakis, Polariton condensation in an optically induced two-dimensional potential, Phys. Rev. B **88**, 041308(R) (2013).